# DESIGN OF ADAPTIVE FUZZY FRACTIONAL ORDER PID CONTROLLER FOR AUTONOMOUS UNDERWATER VEHICLE (AUV) IN HEADING AND DEPTH ATTITUDES

(DOI No: 10.3940/rina.ijme.2016.a1.347)

**M H Khodayari**, and **S Balochian**, Department of Electrical Engineering, Gonabad Branch, Islamic Azad University, Gonabad / Khorasan-e-Razavi, Iran

**SUMMARY**

This paper deals with the design of new self-tuning Fuzzy Fractional Order PID (AFFOPID) controller based on nonlinear MIMO structure for an AUV in order to enhance the performance in both transient state and steady state of traditional PID controller. It is particularly advantageous when the effects of highly nonlinear processes, like high maneuver, parameters variation, have to be controlled in presence of sensor noises and wave disturbances. Aspects of AUV controlling are crucial because of Complexity and highly coupled dynamics, time variety and difficulty in hydrodynamic modeling. In this try, the comprehensive nonlinear model of AUV is derived through kinematics and dynamic equations. The scaling factor of the proposed AFFOPID Controller is adjusted online at different underwater conditions. Combination of adaptive fuzzy methods and $PI^{\lambda}D^{\mu}$ controllers can enhance solving the uncertainty challenge in the PID parameters and AUV parameter uncertainty. The simulation results show that developed control system is stable, competent and efficient enough to control the AUV in path following with stabilized and controlled speed. Obtained results demonstrate that the proposed controller has good performance and significant robust stability in comparison to traditional tuned PID controllers.

## 1. INTRODUCTION

An Autonomous Underwater Vehicle is a robotic device that is driven through the water by means of a propulsion system, controlled and piloted by an internal processor. AUVs are increasingly used within the maritime industries for different missions including dangerous missions. These include pipeline,oil industry, underwaterstructure inspection, survey on underwater animals and plants, environmental monitoring, chemical plume tracing [1], and so on [2].

The significance of AUVs can be easily found if the UUV plan of the USA marine is investigated [3]. Waves and currents are two basic environmental factor groups that are generally treated as external disturbance in AUV designing. Sensor measurement in this environment is also vulnerable to noise. AUV's dynamicparameters are hard to be calculated and predicted properly using previous state, because of variety of these coefficients in different situations. Moreover, it needs practical tests like two tank test [4] and underwater tests for validation [5, 6]. Hence it seems that self-adaptivity and robustness are exigencies. In particular, we will discuss a special type of PID controller named Adaptive Fuzzy Fractional Order PID (AFFOPID) that combines the advantages of fractional PID [30] control and self-tuning fuzzy logic control.

Using two more degrees of freedom in fractional order PID controller comapred to ordinary PID controller we can improve our desired tasks in control accuracy, power consumption, rise time and robustness depending on different situations. If we can reduce the overshoot, undershoot and the settling time of response to acceptable amounts, the power consumption decreases. Moreover, from controlling aspect, this method is not comparable to PID controller especially in presence of noise and disturbances. Nowadays, implementation of fuzzy logic is a routine procedure and owing to new ARM microcontroller implementations of PID controller and FOPID (Fractional Order PID) are not very different from each other. It means that with simple microcontroller like ARM-1788 it can be implemented with good margins in processing and reliability.

## 2. CONTROL BACKGROUND

Throughout the years researchers have diversified control algorithms for AUV. They proposed algorithms such as: doubled PID, optimized PID, adaptive methods, fuzzy method, robust control, SMC, neural network control, and some hybrid models. For more detail, this includes linear controllers [1, 7-10, 28] which performed satisfactorily, SMC controllers [11, 13], adaptive control [12-13], FLC [14], predictivecontrol [18-21,31] and combination of SMC and adaptive and neural-network-based control [15-17] have also shown good robustness and tuning ability.

All algorithms have some pros and cons, but using hybrid controllers including classical and modern intelligent methods, a suitable controller will be available [25].

PID controller is the most popular industrial controller because of its simplicity and ability to be tuned utilizing few parameters [4]. However, tuning might be challenge according to its situation and desireable changes.Well-developed linear controllers may not be suitable enough for AUV due to the complexities involved in the dynamics of the system and variations of AUV parameters in unsuitable environmental conditions.

Fractional calculus is a field of mathematical analysis which studies the ability of taking real number power of the differential operator and integration operator. The well-established definitions include the Grunwald–Letnikov definition, the Riemann–Liouville definition, and the Caputo definition. Today, fractional calculus is a hot

 

topic which has drawn lots of attentions from almost every branch of modern science [33]. The performance of the PID controller can be improved using fractional order derivatives and integrals. This flexibility helps the robustness. It can be expected that the $PI^{\lambda}D^{\mu}$ controller may enhance the systems control performance [30]. One of the most important advantages of the $PI^{\lambda}D^{\mu}$ controller is less sensitivity to parameter variations of the plan. Therefore, FOPID controller generalizes the PID controller and makes it more flexibe such that controller planning might be apprpriately implemented and we can control the actual processes more accurately.

Adaptive method is a useful method for AUV controlling due to variation of model parameters in the sea. The controller can adapt itself according to smooth waves and currents or weight reduction; however, adaptive control may fail when the velocity of dynamic variation exceeds its adapting capability, and the model-based adaptive control calculation would fail because of the excessive endeavour in system identification.

The fuzzy logic control (FLC) is easy to use in industrial process because of its simple control structure, easy to design and cheap [29]; however, FLC with fixed scaling factors and fuzzy rules may not provide proper performance if the controlled plant has uncertainty and high nonlinearity [14, 23]. Traditional FLC does not oeprate properly in steady state, if the system does not have an inherent integrating property. However, determining the linguistic rules and the membership functions require experimental data and is very time-consuming, and the rule-based structure of fuzzy logic control makes it difficult to characterize the behaviour of the closed-loop system in order to determine response time and stability.

It is not easy to model the AUV characteristics easily and accurately, hence, it is desireable to have a control design which does not require the explicit details of the dynamic model and has a self- adaptive capability so that it can handle parameter variations. Considering its benefits fractional order fuzzy PID controller is a good option [34].

The main goal of this work is to develop a control system for an AUV based on REMUS100 model combining an adaptive fuzzy method and fractional order PID controller. One of the most important advantages of adaptive fuzzy PID controller is that the exact model of system is not necessary and in different situations it can adapt itself [32]. It means that controller compensates for uncertainty modeling. This work is carried out in 4 stages:

1. Deriving REMUS100 nonlinear model in MATLAB2014b/SIMULINK.
2. Implementation of double PID controller in REMUS100 model as an initial controller in three channels; depth, heading and surge.
3. Implementation of AFFOPID controller.
4. Comparing and analyzing 3 types (classical PID, FOPIDandAFFOPID (Adaptive Fuzzy Fractional Order PID)) of controllers in presence of big environmental disturbances and sensor noise.

The rest of the paper is organized as follows. Section 3 deals with a brief discussion about dynamic equations and modeling (preliminary). Sections 4 and 5 represent control methodology. In Section 6, the comparative simulation results and analysis of robustness of the controllers are presented. The paper is concluded in section 7.

## 3. PRELIMINARY

### 3.1 COORDINATE SYSTEMS AND KINEMATIC- DYNAMIC EQUATIONS

Generally, the motion of an AUV can be introduced using six degrees of freedom (6-DOF) differential equations of motion [4, 27]. These equations are developed using two coordinate frames (Figure.1). Six velocity components [*u, v, w, p, q, r*] (surge, sway, heave, roll rate, pitch rate, yaw rate) are defined in body-fixed frame while the earth-fixed frame defines the corresponding attitudes and positions [x, y, z, $\varphi$, $\theta$ and $\psi$ ]. This is presented in Table.1 and Figure.1.

The sense of the axis is right-handed; hence *x*-axis is positive forward, *y*-axis is positive to starboard, *z*-axis is positive down, $\theta$ is positive nose-up, $\varphi$ is positive clockwise and $\psi$ is positive to starboard. The origin of the body-fixed coordinate system is $[X_{cg} = 0.00m \quad Y_{cg} = 0.00m \quad Z_{cg} = 1.96e-002]$

Table.1. Symbols of 6-DOF

| *DOF* | *Motion* | *Forces and Moments* | *Linear and Angular velocity* | *Positions and Euler Angles* |
|---|---|---|---|---|
| *1* | *Surge* | *X(N)* | *u(m.s$^{-1}$)* | *x(m)* |
| *2* | *Sway* | *Y(N)* | *v(m.s$^{-1}$)* | *y(m)* |
| *3* | *Heave* | *Z(N)* | *w(m.s$^{-1}$)* | *z(m)* |
| *4* | *Roll* | *K(N.m)* | *p(rad. s$^{-1}$)* | $\phi(rad)$ |
| *5* | *Pitch* | *M(N.m)* | *q(rad. s$^{-1}$)* | $\theta(rad)$ |
| *6* | *Yaw* | *N(N.m)* | *r(rad. s$^{-1}$)* | $\psi(rad)$ |

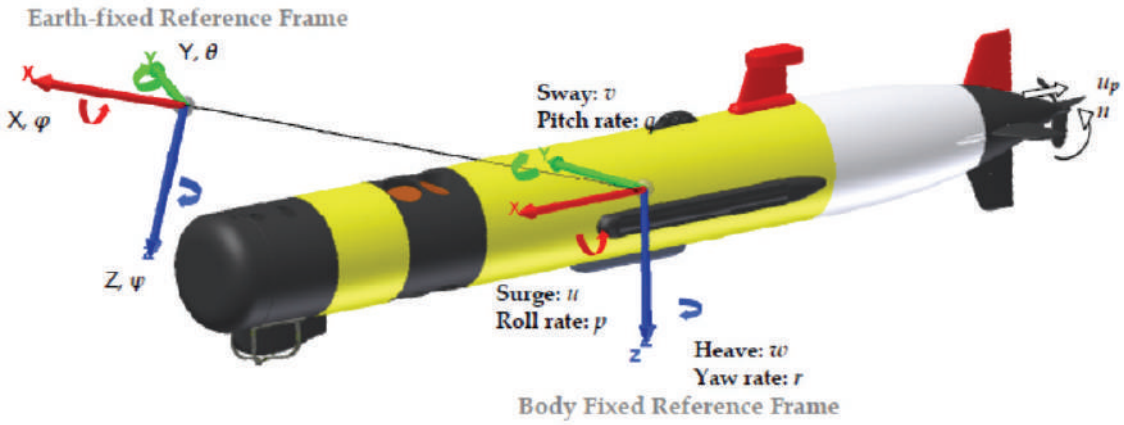


Figure.1.Reference frame of AUV

In this case there are two important coordinate systems, world (earth) coordinates and body coordinates. For marine vehicles it is usually assumed that the acceleration of a point on the surface of earth can be neglected. Thus, an earth fixed frame can be considered to be an inertial frame. This suggests that the linear and angular velocities of the vehicle should be expressed in body-fixed frame while position and orientation should be described with respect to inertial frame [12]. There are some processes which must be modeled in the simulation including the vehicle hydrodynamics, rigid body dynamics, and actuator dynamics, etc.

The AUV motion vectors:

$\boldsymbol{\eta}_1 = [x \quad y \quad z]^T$ *position vector*,

$\boldsymbol{\eta}_2 = [\phi \quad \theta \quad \psi]^T$ *Euler angles vector*

$\boldsymbol{v}_1 = [u \quad v \quad w]^T$ *linear velocity vector*,

$\boldsymbol{v}_2 = [p \quad q \quad r]^T$ *angular velocity vector*

$\boldsymbol{\tau}_1 = [X \quad Y \quad Z]^T$ *forces vector*

$\boldsymbol{\tau}_2 = [K \quad M \quad N]^T$ *moments vector*

Transformation between these two coordinate systems is as follows,

$$J_1(\eta_2) = C^T_{z,\psi}.\, C^T_{y,\theta}.\, C^T_{x,\varphi} = \begin{bmatrix} \cos(\psi) & -\sin(\psi) & 0 \\ \sin(\psi) & \cos(\psi) & 0 \\ 0 & 0 & 1 \end{bmatrix} \begin{bmatrix} \cos(\theta) & 0 & \sin(\theta) \\ 0 & 1 & 0 \\ -\sin(\theta) & 0 & \cos(\theta) \end{bmatrix} \begin{bmatrix} 1 & 0 & 0 \\ 0 & \cos(\phi) & -\sin(\phi) \\ 0 & \sin(\phi) & \cos(\phi) \end{bmatrix} \quad (1)$$

For speed transformation, by this matrix equation the three world coordinate frame translations rates can be obtained from the body coordinate frame translation rates (Eq.2).

$$\begin{bmatrix} \dot{x} \\ \dot{y} \\ \dot{z} \end{bmatrix} = J_1(\eta_2).\begin{bmatrix} u \\ v \\ w \end{bmatrix} \quad (2)$$

Inversely, body coordinate frame velocities can be determined from world coordinate frame velocities in a similar fashion (Eq.3):

$$\begin{bmatrix} u \\ v \\ w \end{bmatrix} = \left[J^{-1}{}_1(\eta_2)\right]\begin{bmatrix} \dot{x} \\ \dot{y} \\ \dot{z} \end{bmatrix} \quad (3)$$

where:

$$J_1(\eta_2) = \begin{bmatrix} \cos\theta.\cos\psi & \sin\varphi.\sin\theta.\cos\psi - \cos\varphi.\sin\psi & \cos\varphi.\sin\theta.\cos\psi + \sin\varphi.\sin\psi \\ \cos\theta.\sin\psi & \sin\varphi.\sin\theta.\sin\psi + \cos\varphi.\cos\psi & \cos\varphi.\sin\theta.\sin\psi - \sin\varphi.\cos\psi \\ -\sin\theta & \sin\varphi.\cos\theta & \cos\varphi.\cos\theta \end{bmatrix} \quad (4)$$

From body coordinate rotation rates the Euler angle rotation rates are obtained using the following non-orthogonal linear transformations. These three angles are as follows (Eq.5, 6 and 7):

$$\dot{\varphi} = p + q\sin(\varphi)\tan(\theta) + r\cos(\varphi)\tan(\theta) \quad (5)$$

$$\dot{\theta} = q\cos(\varphi) - r\ \sin(\varphi) \quad (6)$$

$$\dot{\psi} = \frac{q\sin(\varphi) + r\cos(\varphi)}{\cos(\theta)} \quad (7)$$

These three equations might be denoted in matrix notation forms as shown by undergoing equation (Eq.8):

$$\begin{bmatrix} \dot{\varphi} \\ \dot{\theta} \\ \dot{\psi} \end{bmatrix} = J_2(\eta_2).\begin{bmatrix} p \\ q \\ r \end{bmatrix} \quad (8)$$

where:

$$J_2(\eta_2) = \begin{bmatrix} 1 & \sin(\varphi)\tan(\theta) & \cos(\varphi)\tan(\theta) \\ 0 & \cos(\varphi) & -\sin(\varphi) \\ 0 & \sin(\varphi)\sec(\theta) & \cos(\varphi)\sec(\theta) \end{bmatrix} \quad (9)$$

and the angular velocity from Euler angular rates are as follows (Eq.10):

$$\begin{bmatrix} p \\ q \\ r \end{bmatrix} = J_2^{-1}(\eta_2)\begin{bmatrix} \dot{\varphi} \\ \dot{\theta} \\ \dot{\psi} \end{bmatrix} \quad (10)$$

where:

$$J_2^{-1}(\eta_2) = \begin{bmatrix} 1 & 0 & -\sin(\theta) \\ 0 & \cos(\varphi) & \sin(\varphi)\cos(\theta) \\ 0 & -\sin(\varphi) & \cos(\varphi)\cos(\theta) \end{bmatrix} \quad (11)$$

Combined speed matrix definitions are as follows in matrix notation:

Finally:

$$\dot{\eta} = J(\eta_2).\nu \quad \Leftrightarrow \quad \begin{bmatrix} \dot{\eta}_1 \\ \dot{\eta}_2 \end{bmatrix} = \begin{bmatrix} J_1(\eta_2) & 0_{3\times3} \\ 0_{3\times3} & J_2(\eta_2) \end{bmatrix}\begin{bmatrix} \nu_1 \\ \nu_2 \end{bmatrix} \quad (12)$$

$$[V]_{world} = [J(\eta_2)]\,[V]_{body} = \begin{bmatrix} J_1(\eta_2) & 0 \\ 0 & J_2(\eta_2) \end{bmatrix}[V]_{body} \quad (13)$$

$$[V]_{body} = [J(\eta_2)]^{-1}[V]_{world} = \begin{bmatrix} [J_1(\eta_2)]^T & 0 \\ 0 & [J_2(\eta_2)]^{-1} \end{bmatrix}[V]_{world} \quad (14)$$

## 3.2 DYNAMICS

Center of buoyancy and mass are repredented as: $r_G = [x_G, y_G, z_G]^T$ $r_B = [x_B, y_B, z_B]^T$.

External forces and moments are obtained according to [4]. The external forces acting on the rigid body of AUV are composed of hydrostatic forces, hydrodynamic forces and forces due to the control surfaces and propeller; that is

$$\sum F_{ext} = F_{hydrostatic} + F_{lift} + F_{drag} + F_{control} + F_{disturbances} \quad (15)$$

According to Newton-Euler formulation, the 6-DOF rigid-body equations of motion in the body-fixed coordinate are as shown below:

$$m\left[\dot{u} - vr + wq - x_G\left(q^2 + r^2\right) + y_G\left(pq - \dot{r}\right) + z_G\left(pr + \dot{q}\right)\right] = X \quad (16)$$

$$m\left[\dot{v} - wp + ur - y_G\left(r^2 + p^2\right) + z_G\left(pr - \dot{p}\right) + x_G\left(qp + \dot{r}\right)\right] = Y \quad (17)$$

$$m\left[w - uq + vp - z_G\left(p^2 + q^2\right) + x_G\left(rp - q\right) + y_G\left(rq + \dot{p}\right)\right] = Z \quad (18)$$

$$I_{xx}\dot{p} + \left(I_{zz} - I_{yy}\right)qr + m\left[y_G\left(\dot{w} - uq + vp\right) - z_G\left(\dot{v} - wp + ur\right)\right] = K \quad (19)$$

$$I_{yy}\dot{q} + \left(I_{xx} - I_{zz}\right)rp + m\left[z_G\left(\dot{u} - vr + wq\right) - x_G\left(\dot{w} - uq + vp\right)\right] = M \quad (20)$$

$$I_{zz}\dot{r} + \left(I_{yy} - I_{xx}\right)pq + m\left[x_G\left(\dot{v} - wq + ur\right) - y_G\left(\dot{u} - vr + wq\right)\right] = N \quad (21)$$

The first three equations (Eqs.16, 17 and 18) are related to external forces for direct motion and the rest of them (Eqs.19, 20 and 21) correspond to rotational motion. Schematic of forces and moments is illustrated in Figure.2.

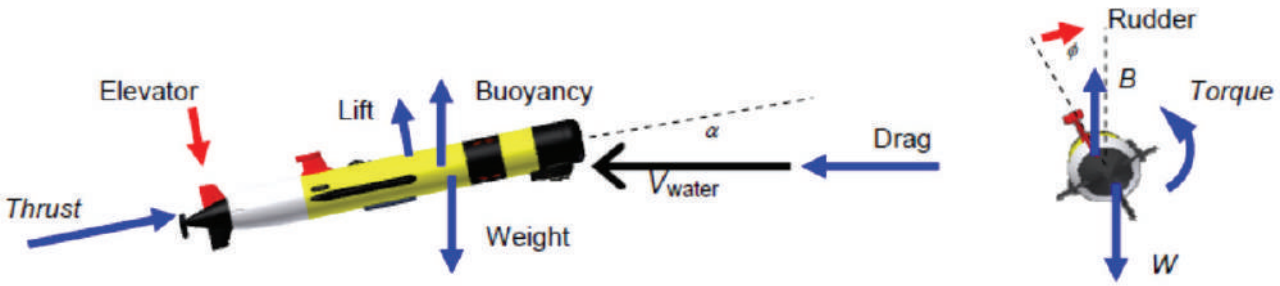


Figure.2. External forces and moments

The buoyant (B) and weight (W) components are acting in the global vertical direction and they must be transformed into components in the vehicle fixed frame in order to be added to the equations of motion.

$$f_G(\eta_2) = J_1^{-1}\begin{bmatrix}0\\0\\W\end{bmatrix} \tag{22}$$

$$f_B(\eta_2) = J_1^{-1}\begin{bmatrix}0\\0\\B\end{bmatrix} \tag{23}$$

The hydrostatic forces and moments on the vehicle can be explained as:

$$F_{HS(hydrostatic)} = f_G - f_B \tag{24}$$

$$M_{HS(hydrostatic)} = r_G \times f_G - r_B \times f_B \tag{25}$$

These equations can be expanded so that nonlinear equations for hydrostatic forces and moments are yielded:

$$\begin{bmatrix}F_{hydrostatic}\\M_{hydrostatic}\end{bmatrix} = -\begin{bmatrix}(W-B)s\theta\\-(W-B)c\theta\ s\phi\\-(W-B)c\theta\ s\phi\\-(y_GW-y_BB)c\theta\ c\varphi+(z_GW-z_BB)c\theta\ s\phi\\(z_GW-z_BB)s\theta+(x_GW-x_BB)c\theta\ c\phi\\-(x_GW-x_BB)c\theta\ s\phi-(y_GW-y_BB)s\theta\end{bmatrix} \tag{26}$$

Eq.26 can be added to the right hand side of the equations of motion in Eqs.16-21. Considering the effect of other forces and moments such as roll drag, axial and lateral of body, body lift and moment, axial and lateral add mass effect, roll added mass, actuator lifts and propeller forces according to [4 and 27-28] total equation is achieved. Exploiting these angle rates and accelerations, the position of AUV will be available.

$$\sum X_{ext} = X_{HS} + X_{u|u|}u|u| + X_{\dot{u}}\dot{u} + X_{wq}wq + X_{qq}qq + X_{vr}vr + X_{rr}rr + X_{prop} \tag{27}$$

$$\sum Y_{ext} = Y_{HS} + Y_{v|v|}v|v| + Y_{r|r|}r|r| + Y_{\dot{r}}\dot{r} + Y_{\dot{v}}\dot{v} + Y_{ur}ur + Y_{wp}wp + Y_{pq}pq + Y_{uv}uv + Y_{uu\delta_r}u^2\delta_r \tag{28}$$

$$\sum Z_{ext} = Z_{HS} + Z_{w|w|}w|w| + Z_{q|q|}q|q| + Z_{\dot{w}}\dot{w} + Z_{\dot{q}}\dot{q} + Z_{uq}uq + Z_{vp}vp + Z_{rp}rp + Z_{uw}uw + Z_{uu\delta_s}u^2\delta_s \tag{29}$$

$$\sum K_{ext} = K_{HS} + K_{p|p|}p|p| + K_{\dot{p}}\dot{p} + K_{prop} \tag{30}$$

$$\sum M_{ext} = M_{HS} + M_{w|w|}w|w| + M_{q|q|}q|q| + M_{\dot{w}}\dot{w} + M_{\dot{q}}\dot{q} + M_{uq}uq + M_{vp}vp + M_{rp}rp + M_{uw}uw + M_{uu\delta_s}u^2\delta_s \tag{31}$$

$$\sum N_{ext} = N_{HS} + N_{v|v|}v|v| + N_{r|r|}r|r| + N_{\dot{r}}\dot{r} + N_{\dot{v}}\dot{v} + N_{ur}ur + N_{wp}wp + N_{pq}pq + N_{uv}uv + N_{uu\delta_r}u^2\delta_r \tag{32}$$

According to (Eqs16-26)

$$m[\dot{u} - vr + wq - x_g(q^2 + r^2) + y_g(pq - \dot{r}) + z_g(pr + \dot{q})] =$$
$$X_{HS} + X_{u|u|}u|u| + X_{\dot{u}}\dot{u} + X_{wq}wq + X_{qq}qq + X_{vr}vr + X_{rr}rr + X_{prop} \quad (33)$$

$$m[\dot{v} - wp + ur - y_g(r^2 + p^2) + z_g(qr - \dot{p}) + x_g(qp + \dot{r})] =$$
$$Y_{HS} + Y_{v|v|}v|v| + Y_{r|r|}r|r| + Y_{\dot{r}}\dot{r} + Y_{\dot{v}}\dot{v} + Y_{ur}ur + Y_{wp}wp + Y_{pq}pq + Y_{uv}uv + Y_{uu\delta_r}u^2\delta_r \quad (34)$$

$$m[\dot{w} - uq + vp - z_g(p^2 + q^2) + x_g(rp - \dot{q}) + y_g(rq + \dot{p})] =$$
$$Z_{HS} + Z_{w|w|}w|w| + Z_{q|q|}q|q| + Z_{\dot{w}}\dot{w} + Z_{\dot{q}}\dot{q} + Z_{uq}uq + Z_{vp}vp + Z_{rp}rp + Z_{uw}uw + Z_{uu\delta_s}u^2\delta_s \quad (35)$$

$$I_{xx}\dot{p} + (I_{zz} - I_{yy})qr + m[y_g(\dot{w} - uq + vp) - z_g(\dot{v} - wp + ur)] =$$
$$K_{HS} + K_{p|p|}p|p| + K_{\dot{p}}\dot{p} + K_{prop} \quad (36)$$

$$I_{yy}\dot{q} + (I_{xx} - I_{zz})rp + m[z_g(\dot{u} - vr + wq) - x_g(\dot{w} - uq + vp)] =$$
$$M_{HS} + M_{w|w|}w|w| + M_{q|q|}q|q| + M_{\dot{w}}\dot{w} + M_{\dot{q}}\dot{q} + M_{uq}uq + M_{vp}vp + M_{rp}rp + M_{uw}uw + M_{uu\delta_s}u^2\delta_s \quad (37)$$

$$I_{zz}\dot{r} + (I_{yy} - I_{xx})pq + m[x_g(\dot{v} - wp + ur) - y_g(\dot{u} - vr + wq)] =$$
$$N_{HS} + N_{v|v|}v|v| + N_{r|r|}r|r| + N_{\dot{r}}\dot{r} + N_{\dot{v}}\dot{v} + N_{ur}ur + N_{wp}wp + N_{pq}pq + N_{uv}uv + N_{uu\delta_r}u^2\delta_r \quad (38)$$

Finally after sorting one may write:

$$\begin{bmatrix} m - X_{\dot{u}} & 0 & 0 & 0 & mz_g & -my_g \\ 0 & m - Y_{\dot{v}} & 0 & 0 & 0 & mx_g - Y_{\dot{r}} \\ 0 & 0 & m - Z_{\dot{w}} & my_g & -mx_g - Z_{\dot{q}} & 0 \\ 0 & -mz_g & my_g & I_{xx} - K_{\dot{p}} & 0 & 0 \\ mz_g & 0 & -mx_g - M_{\dot{w}} & 0 & I_{yy} - M_{\dot{q}} & 0 \\ -my_g & mx_g - N_{\dot{v}} & 0 & 0 & 0 & I_{zz} - N_{\dot{r}} \end{bmatrix} \begin{bmatrix} \dot{u} \\ \dot{v} \\ \dot{w} \\ \dot{p} \\ \dot{q} \\ \dot{r} \end{bmatrix} = \begin{bmatrix} \sum X \\ \sum Y \\ \sum Z \\ \sum K \\ \sum M \\ \sum N \end{bmatrix} \quad (39)$$

## 4. CONTROL METHODOLOGY

AUV movement in the water is handled by propeller system and fin surfaces.The REMUSE100 AUV control system uses two twin rudder fins and two twin elevators (stern) fins. The device is controlled through controlling propellers and fin deflections. For completeness, this work presents three main control schemes and implements them in the plan. These consist of traditional PID, FOPID and AFFOPID.

Overall, in this case there are 3 goals that require to be improved:

1. Depth control
2. Steering (heading) control
3. Forward velocity (surge ($u$))

### 4.1 MODELING

Initial values are considered according to Table.2:

This model is nonlinear and has complex coupling between the degrees of freedom. Desired model has 3 inputs and 3 outputs. System has 12 states $\chi = [u \quad v \quad w \quad p \quad q \quad r \quad x \quad y \quad z \quad \phi \quad \theta \quad \varphi]$.

Coupling between the degrees of freedom should be considered correctly and rationally. Inputs are considered to be $[X_{prop} \quad \delta_s \quad \delta_r]$ and outputs are $[x \quad y \quad z]$ (initial MIMO structure). The model includes 1 sub-block where nonlinear equations with an integral function (with initial condition*u=1.54m/s*; ([1.54×1 0 0 0 0 0 0 0 0 0 0 0]') has been used. In this sub-block all velocities and accelerations are calculated and obtained according to nonlinear equations.

After modeling, the validation of open-loop results has been compared with good standing reference [4]. The comparison revealed that the modeling is very near to these references for REMUSE100. For example the Euler angels and their rates are investigated according to Figure. 3 and Figure. 4, respectively. The open loop simulation results are very near to reference [4].

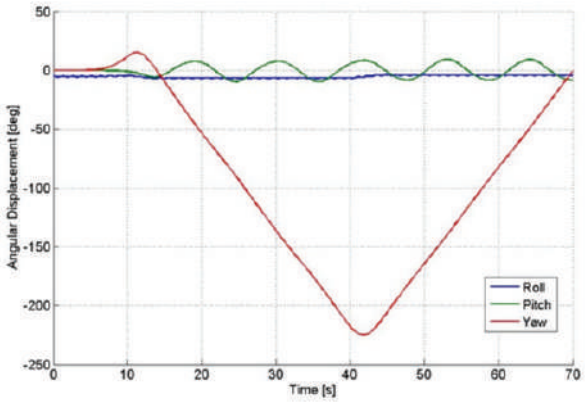


Figure.3. Euler angels in our open-loop model the same as Ref [4]

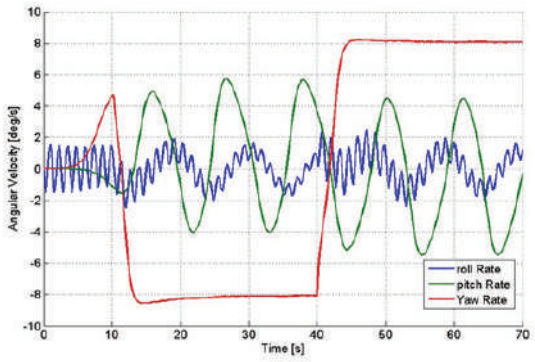


Figure.4. Angular speedin our open-loop model the same as Ref [4]

## 4.2 DOUBLE PID CONTROLLER

### 4.2.(a) Speed controller

According to rational assumption and ignoring minor interaction between surge, heave, sway, pitch, roll, and yaw, it seems that a proportional controller ($k_p$) is sufficient for propeller. The main equation is

$$X_{prop} = -X_{u|u|}u|u| = -2.28X_{u|u|} \tag{40}$$

Where $X_{u|u|} = -1.62\ Kg.m^{-1}$

Where $X_{u|u|}$ is the axial drag coefficient– resisting forward motion [27].

Moreover, $K_{prop}$ that describes the moment of motor is achievable in this model. The main equation is as follows:

$$\begin{aligned} K_{prop} &= K_{HS} \\ &= (y_g W - y_b B)\cos\theta\cos\phi + \\ &+ (z_g W - z_b B)\cos\theta\sin\phi \\ &= 0.995\ (y_g W - y_b B) - 0.093(z_g W - z_b B) \end{aligned} \tag{41}$$

The value of $k_p$ is chosen such that acceptable level of performance is acheived. According to SIMULINK tuning the suitable choice for the gain is $K_p$=10.08. According to our simulation, the stabilized speed reaches to 1.27 m/s.

### 4.2.(b) PID controller for Depth and Heading attitude

The couplings between *Z*-axis and pitch as well as *Y*-axis and yaw are very strong. In other worlds, according to nonlinear equations, it is not possible to control them independently. Moreover, from another aspect, the independency of two channels (heading and depth) should be investigated, as well.

In this paper almost the control strategy of both channels is identical. The main dependency in depth channel is related to heave velocity $\omega(t)$, pitch rate $q(t)$, pitch angle $\theta(t)$, and the depth $z(t)$. In heading channel the main parameter depends on heave velocity $v(t)$, yaw rate $r(t)$, yawangle $\psi(t)$, and $y(t)$. The control variable is the deflection angle of stern planes $\delta_s(t)$ and $\delta_r(t)$ for depth control and heading control, respectively.

In this work approximating AUV equations, ignoring minor sentences and the relationship between parameters the control of depth limits to control of $\theta$ and $z$ while the control of heading limits to control of $\psi$ and $y$. In this way main MIMO structure is in this fashion: using three inputs ($\begin{bmatrix} X_{prop} & \delta_s & \delta_r \end{bmatrix}$), control of two outputs $z$ and $y$ is achievable.

Table.2. Some of main used parameters

| *Parameters* | *Values* | used equations |
|---|---|---|
| *Initial surge velocity(u)* | *1.54m/s* | Eq.2,3,16-21,27-39 |
| *Xprop* | *3.861N* | Eq.33,40 |
| *Kprop* | *0N.m* | Eq.36,41 |
| *Motor* | *1500RPM* | |
| *Weight* | *2.99e2N* | Eq.16-18(m),22,26,33-38,41 |
| *Buoyancy* | *2.99e2N* | Eq.23,26,41 |
| $z_B$ | *0m* | Eq.41,26 |
| $x_B$ | *0m* | Eq.26 |
| $y_B$ | *0m* | Eq.41,26 |
| $z_G$ | *0.0196m* | Eq.26,39,41 |
| $x_G$ | *0m* | Eq.26 |
| $y_G$ | *0m* | Eq.26,41 |
| $I_{xx}$ | $0.177kg.m^2$ | Eq.19,35,36 |
| $I_{yy}$ | $3.45\ kg.m^2$ | Eq.20,35,36 |
| $I_{zz}$ | $3.45\ kg.m^2$ | Eq.21,35,36 |

 

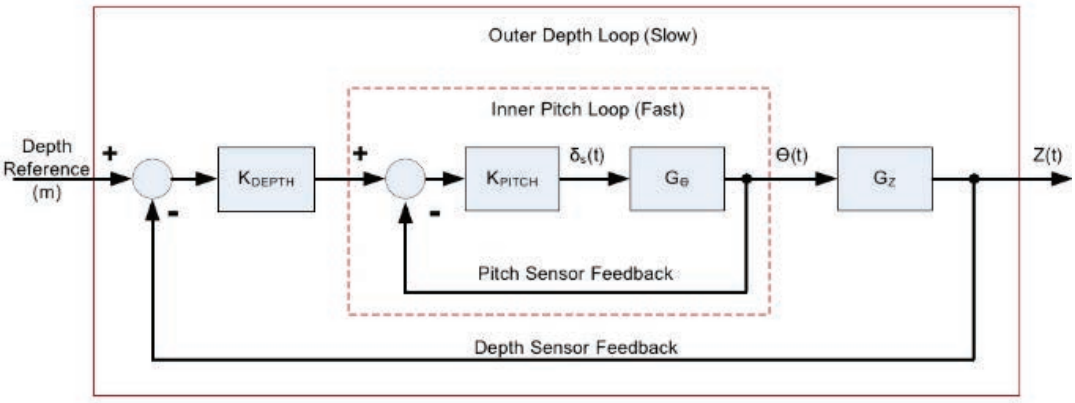


Figure.5. Main block diagram of a depth controller in double PID strategy

In other words, the control can be divided into two independent planes. Each plane has an inner and outer loop. For example in depth we adopt dual loop control methodology by means of an inner pitch control loop and an outer depth control loop. In the dual loop methodology, the depth controller generates a desired pitch angle which becomes the input to the pitch controller. Then, the pitch controller handles the elevator deflection $\delta_s$, based on the proper pitch angle. This idea is illustrated in Figure.5. The inner plane should be stable and faster than outer plane. Therefore, stability and usual accurate tracking are enough for an inner PID loop. This can be done using classical methods or employing parameter tuning through increasing the loop speed. Therefore, further improvement was not required. Finally, each plane can be tuned through tuning outer loop using classical Zeigler-Nichols rules.

It should be mentioned that after investigating inner loop and obtaining transfer functions, it was revealed that both channels (inner loop of z and y channels) have zeros on the right side of imaginary axis; thus, we have two non-minimum phase system necessitating proper control strategy selection.

The block diagram of total classical control method in SIMULINK is depicted in Figure. 7.

To obtain more realistic simulations, in this model the boundary of fins is limited between -10°~ +10° and implemented using saturation functions before actuator inputs. The simulation results are demonstrated in Figure. 6.

Table.3.Classical PID parameters

| Coefficient/ channel | $\varphi$ | $y$ | $\theta$ | $z$ |
|---|---|---|---|---|
| $k_p$ | -4.9761 | 0.16742 | -6 | -0.2803285 |
| $k_I$ | -0.32442 | 0.0003153 | -0.1 | -0.000829 |
| $k_D$ | -4.934 | -0.45 | -9 | 0.47021093 |
| Filter coefficient (N) | 21.6765 | 0.30459 | 10.6636 | 0.47859 |

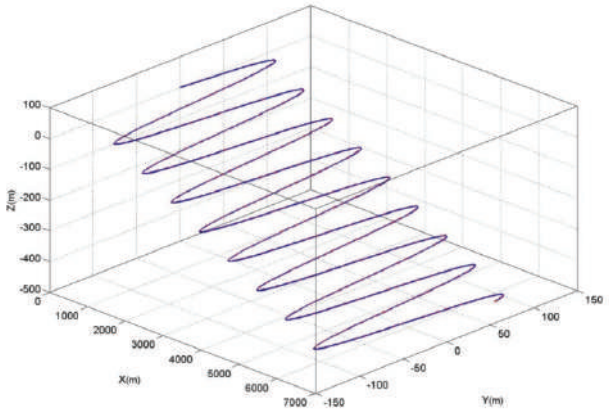


Figure.6. 3-D Trajectory following in $z$ and $x$-$y$ simultaneously in dual PID controller y = 100sin (2pi.t/(60.180)), H = -0.1t;

As we can see in Figure.6, this controller has a good performance in tracking in both channels simultaneously. There is not an excessive effort on fins and tracking (without interaction) has been met in both channels. Controller coefficients are presented in Table.3. For better stability a low pass filter (LPF) in derivative coefficient has been considered in controller. Furthermore, for each channel ($\varphi$,y,$\theta$,z) a PID controller is considered. The filter coefficient (N Coefficient) sets the location of the pole in the derivative filter. For a continuous-time parallel PID controller, the transfer function is:

$$C_{pars} = \left[ K_p + K_I\left(\frac{1}{S}\right) + K_D\left(\frac{NS}{S+N}\right) \right]$$

According to physical structure of REMUSE100 and its symmetrical weight distribution [4], its low speed and its environmental assumptions [4], the AUV is symmetric about the $x$-$z$ plane and close to symmetric about the $y$-$z$ plane. Although the AUV is not symmetric about $x$-$y$ plane it is assumed that it is symmetric about this plane, so we can decouple the degrees of freedom. The AUV can be assumed to be symmetric about three planes since the vehicle operates at low speed. For more details, after of

linearization in Simulink, this transfer matrix was obtained $\begin{bmatrix} \frac{y1}{u1} & \approx 0 \\ \approx 0 & \frac{y2}{u2} \end{bmatrix}$. This MIMO matrix confirms our claim because the transfer function is very near to zero in any frequency on subsidiary diagonal.

In order to obtain the minimum proper period of desired trajectory in both channels the system response in both channels is investigated simultaneously. This shows that almost T=40s is the minimum allowable value gauranteeing proper performance in both channels.

## 5. AFFOPID

In AUV case, traditional PID control design techniques such as empirical Cohen–Coon formula, Ziegler–Nichols, Chien–Hrones–Reswick formula, refined Ziegler–Nichols tuning and Wang–Juang–Chan formula are not useful in presence of parameter variations, nonlinearity and so on.

Two more degrees of freedom in fractional-order integrator and differentiator makes it possible to improve the performance of classical PID controllers. However, tuning is more difficult than traditional PID. The transfer function of PID controller is $G_c(s) = \frac{U(s)}{E(s)} = K_P + \frac{K_i}{S^\lambda} + K_d S^\mu$ where $(1 > \lambda, \mu > 0)$

E(s) is error; U(s) is controller output and $G_c(s)$ is transfer function of controller.

Recently, some software tools in MATLAB such as FOMCON, NINTEGER, and CRONEL are introduced for modeling. In this work FOMCONtoolbox [24, 26] is preferred owing to its advantaged over its counterparts.

In the following, each channel is linearized and the FOPID is implemented. These transfer functions are obtained after linearization (Eq.42 and Eq.43):

In linearization, trim point is defined in this way:
$u = 1.54 m/s \quad v = 0 \quad w = 0 \quad p = 0 \quad q = 0$
$r = 0 \quad x \quad y \quad z \quad \phi = 0 \quad \theta = 0 \quad \varphi = 0$

Note that trim point is a type of equilibrium point and could be defined based on our preferences and requirements.

### 5.1 STRUCTURE OF FOPID

The structure of the fractional order fuzzy PID used here comprise a combination of fractional PID and FLC with two more regulator coefficients (α (Gain4) and β (Gain3)) as input of FLC. These two coefficients give extra flexibility to system control resulting in lower error index and lower control signal. These two parameters could be obtained and optimized for the best performance either using GA algorithm (or some similar methods) or trial and error for best performance. Utilizing two more parameters and the performance might be improved, the role of error and its fractional rate error can be weighted. In fuzzy PID controller, inputs are error signals and the fractional order derivative of error rate multiplied by α and β, respectively. The FLC outputs are added to static coefficient fractional PID controller and make them online. In this model the integer order rate of the error at the input of FLC is replaced with its fractional order counterpart (μ). The $K_P, K_d$ and $K_i$ values together with μ and λ are optimization variables in Nelder-Mead algorithm with ITSE (Integral of Time multiplied Squared Error) and ITAE performance metric, where $ITSE = \int_0^\infty te^2(t)dt$ and $ITAE = \int_0^\infty t|e(t)|\,dt$ and *e(t) = 20(m)− y(t),y(t)* is the output. Comparing ITAE and ITSE, since the absolute error is included in the ITAE criterion, the maximum percentage of overshoot $M_P$ is also minimized. The ITSE criterion penalizes the error more than the ITAE and due to the time multiplication term, the oscillation damps out faster. However, for a sudden change in set-point the ITSE based controller produces larger controller output than the ITAE based controllers, which is not desirable from actuator design point of view. Other integral performance indices like ISTES and ISTSE both have higher powers of time and error terms. These result in faster rise time and settling time while ensuring the minimization of the peak overshoot. These, however, might lead to very high value of control signal and are only used in acute cases where the time domain performance is of critical importance and not a large control signal.

Table.4.Optimization assumption and constraints

| | |
|---|---|
| Desired G.M | 6db |
| Desired PH.M | 60° |
| Approximate order | 5 |
| Approximate as | Oustaloup filter |
| Constraint of $k_p$ | [-100~100] |
| Constraint of $k_i$ | [-100~100] |
| Constraint of $k_d$ | [-100~100] |
| Constraint of $\lambda$ | [0.01~1] |
| Constraint of $\mu$ | [0.01~0.9] |
| Time step | 0.01~0.5 |
| Optimization algorithm | Nelder-Mead |
| Performance index | IAE[1],ISE[2],ITSE[3],ITAE[4] |

[1] Integral of Absolout Error
[2] Integral of Squared Error
[3] Integral of Time multiplied Squared Error
[4] Integral of Time-weighted Absolute Error

5.1.(a) Implementation of fopid:

Exploiting Eqs 42-43 and simulating Nelder-Mead algorithm using desired assumptions and constraints (mentioned in Table.4) the simulation results might be obtained as shown in Table.7.

In this simulation various time domain integral performance indices like ITAE, ITSE, ISTES and ISTSE with their results are considered as presented in Table.5. Besides, other optimization methods like Interior-point and SQP (Sequential Quadratic Programming) are investigated as demonstrated by Table.6. We know that SQP is one of the most successful methods for the numerical solution of constrained nonlinear optimization problems. It relies on a profound theoretical foundation and provides powerful algorithmic tools for solving Large-scale technologically relevant problems. The idea of SQP methods is to solve the nonlinearly constrained problem using a sequence of quadratic programming (QP) sub problems. The constraints of each QP sub problem are linearized version of the constraints in the original problem. Additionally, the objective function of the sub problem is aquadratic approximation of the Lagrangian function.

In FOMCON there are two types of filters (Oustaloup filter and refined Oustaloup filter ) can avoid algebraic loops in Simulink in specified frequency domain $w = [w_b; w_h]$ with order of approximation ($N=5$ is default). A low-pass filter is also used in series with the LTI block with crossover frequency of $1/w_h$ [35].

## 5.2 STRUCTURE OF ADAPTIVE FUZZY

The main scheme of AFFOPIDC with possibility of involving noise and disturbance is depicted in Figure.8. This figure clearly explains the control structure in MATLAM/Simulink. The possibility of including noise and disturbance facilitates obtaining desired and comparable controller with diversity in output. As we can see in Figure.8, all three controllers are implemented; PID, fractional PID AND AFFOPID in bottom-up order.

$$G1 = \frac{Y}{C_1}$$

$$= \frac{-33.29S^8 + 233.4S^7 + 1468S^6 + 8047S^5 + 5.414e004S^4 + 5.97e004s^3 + 1.617e004s^2 + 851.7s}{s^{10} + 26.57s^9 + 312.7S^8 + 2024S^7 + 8672S^6 + 3.342e004S^5 + 3.973e004S^4 + 1.44e004s^3 + 2890s^2 + 147.7s + 0.2686} \quad (42)$$

$$G2 = \frac{Z}{C_2}$$

$$= \frac{30.33S^7 - 63.39S^6 - 801.2S^5 - 1516S^4 - 922.5S^3 - 173.2s^2 - 2.701s}{s^9 + 14.27s^8 + 211.3S^7 + 803.7S^6 + 1191S^5 + 751.1S^4 + 215.7S^3 + 33.37s^2 + 0.5703s + 0.000991} \quad (43)$$

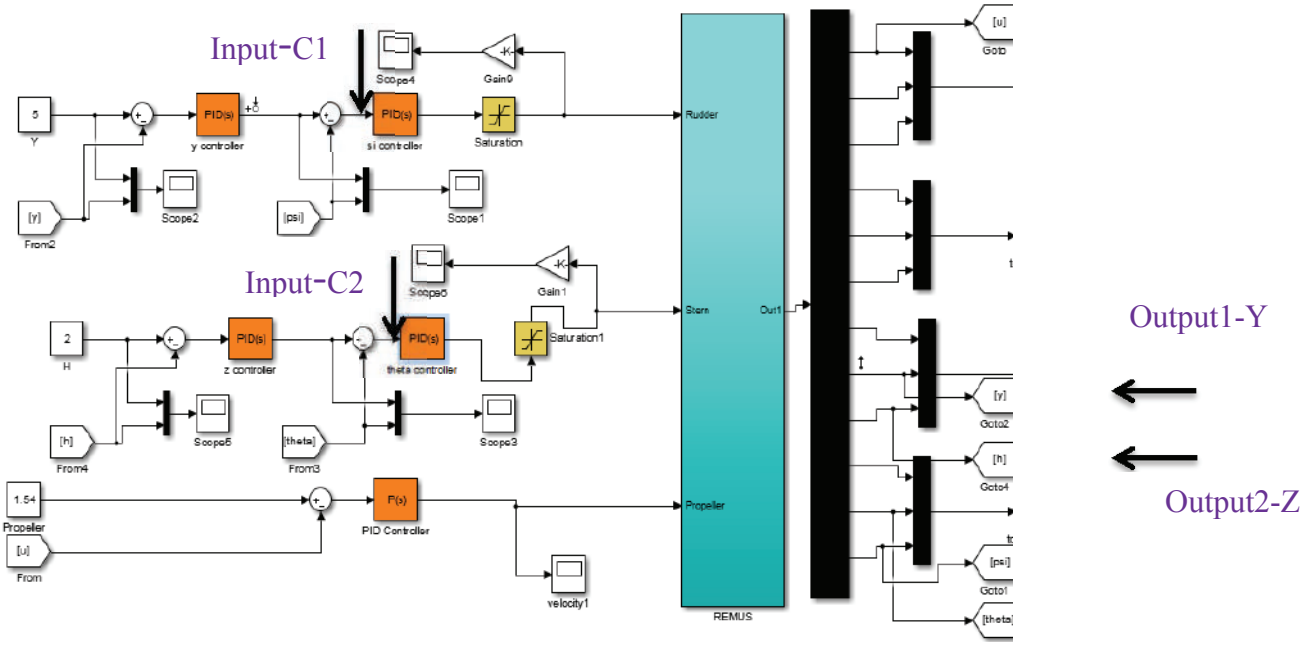


Figure.7. Double PID controller and nonlinear model in Simulink in a very clear form

FOPID controller uses a two dimensional linear rule base for error and error fractional rate.The FLC output combines standard Gaussian and Triangular membership functions and Mamdani type interfacing. The FLC output is determined using center of gravity method with defuzzification.

From implementation and design perspective the triangular function is preferred to other fuzzy memberships in real time operation [33]. All fuzzy sets of the inputs and outputs are NL, NM, NS, ZR, PS, PM, PL that are shown in Figure.9. The FLC is the fuzzy linguistic variables NL, NM, NS, ZR, PS, PM, PL representing Negative Large, Negative Medium, Negative Small, Zero, Positive Small, Positive Medium and Positive Large, respectively. Figure.10 shows the nonlinear surface plot for the rule base of the fuzzy logic controller. In this case only 7 linguistic variables are exploited resulting in 49 rules in Table.8. The set of rules can be divided into the following five cases:

*Assumption 0*: the error and its fractional derivative are minor. This causes process output to get away smoothly from the set point but it is still near to it. Hence small values of control signals are required to correct these small deviations and these rules are mainly related to the steady state treatment.

*Assumption 1*: the error is negative large or medium, dictating that the process output is far above the set point. Also the fractional derivative of the error is positive causing output to move to set point. Hence, controller regulates the speed to reach the set point.

*Assumption 2*:either the error is near to the set point (NS, ZR, and PS) or is much lower (PM and PL). Similarly, since the fractional rate of error is positive, the output is getting away from the set point. Hence, different levels of positive control signal are required for different combinations of $e$ and $\frac{d^{\mu}e}{dt^{\mu}}$, to reverse the trend of output and guides it to the set point.

*Assumption 3*:in this case error is positive medium or big suggesting that output is far below the set point. Simultaneously, since $\frac{d^{\mu}e}{dt^{\mu}}$ is negative, the process output moves to the set point. Thus, controller regulates the speed to reach the set point.

*Assumption 4*: In this group the error is either close to the set point (NS, ZR, and PS) or is much higher (NM, NL). Also since $\frac{d^{\mu}e}{dt^{\mu}}$ is negative the process output variable gets away from the set point. Therefore, a negative control signal reverses this direction and guides the process to the set point.

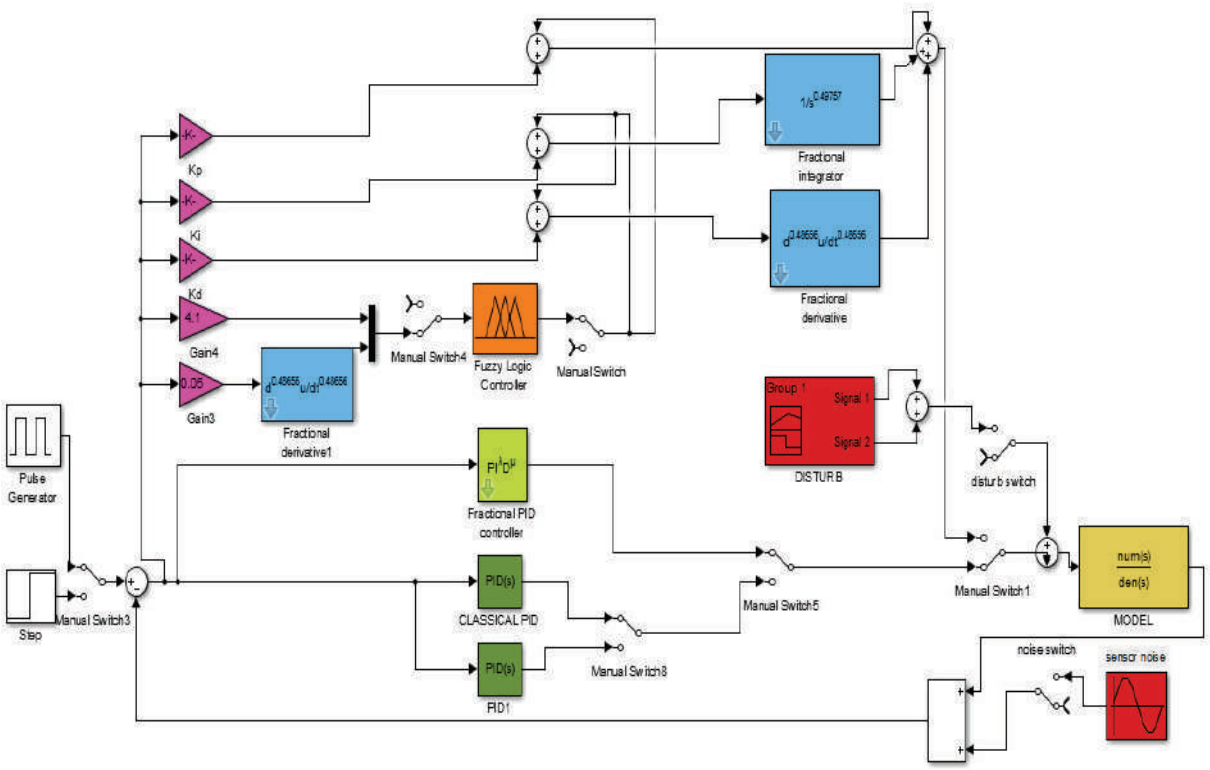


Figure.8. Generic scheme of AFFOPIDC with possibility of including noise and disturbance

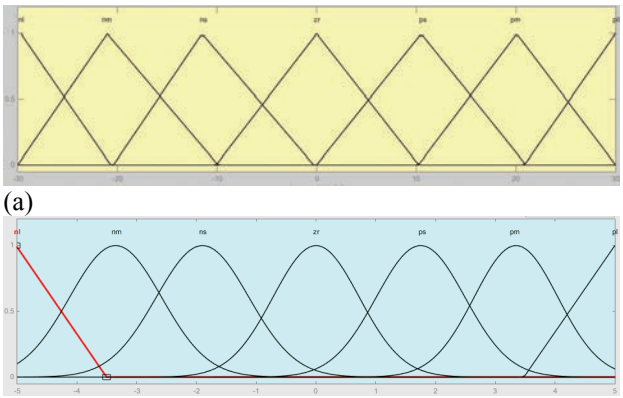

(a)

(b)

Figure.9. Membership functions of FLC. a) Membership functions for error, fractional rate of error and FLC inputs. b) Membership functions of FLC output

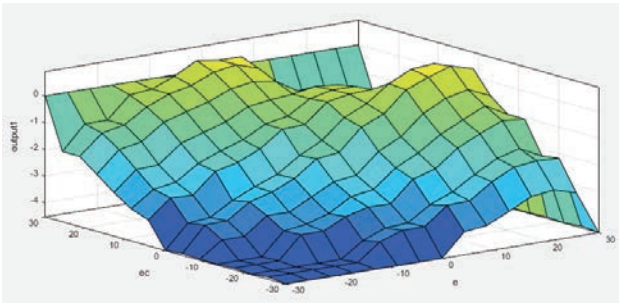

Figure.10.Surface plot of rule base

Table.5. Simulation results of FOPID with comparing different performance indicies

| | $k_p$ | $k_i$ | $k_d$ | $\lambda$ | $\mu$ | G.M | PH.M | $J^{\min}$ |
|---|---|---|---|---|---|---|---|---|
| ITSE | -1.0177 | 1.8789 | 1.0861 | 0.49576 | 0.47899 | 6db | 60.01° | 0.258209 |
| ITAE | -1.8806 | 2.3113 | 1.6234 | 0.49373 | 0.40022 | 5.4339 db | 60° | 11.195325 |
| IAE | -0.42494 | 1.5937 | 0.84364 | 0.50319 | 0.52554 | 6 db | 60° | 1.19639 |
| ISE | 1.0011 | 0.79663 | 0.31054 | 0.6183 | 0.89529 | 6 db | 60.001° | 0.36159 |

Table.6. Simulation result of FOPID with different optimization algorithms

| ITSE | $k_p$ | $k_i$ | $k_d$ | $\lambda$ | $\mu$ | G.M | PH.M |
|---|---|---|---|---|---|---|---|
| Nelder-Mead | -1.0177 | 1.8789 | 1.0861 | 0.49576 | 0.47899 | 6db | 60.01° |
| Interior-point | 1.2924 | 0.40326 | 0.27617 | 0.99972 | 0.89937 | 6.0056 | 63.769 |
| SQP | 0.27407 | 0.59734 | 0.74876 | 0.89252 | 0.34068 | 7.3721 | 62.66 |

Table.7.Result of simulations in Nelder-Mead algorithm for both channels

| Optimized results/constraints | Channel $Y$ | Channel $Z$ |
|---|---|---|
| $k_p$ | -1.0177 | -0.7311 |
| $k_i$ | 1.8789 | -0.69978 |
| $k_d$ | 1.0861 | -0.26777 |
| $\lambda$ | 0.49576 | 0.76696 |
| $\mu$ | 0.47899 | 0.55725 |
| $\alpha$ | 4 | 0.3 |
| $\beta$ | 0.02 | 0.095 |
| Performance metric | ITSE | ITSE |
| Gain margin | 6 | 6 |
| Phase margin | 60.01 | 60 |
| Final error $J^{\min}$ | 0.258209 | 0.19169 |
| Order of approximation | 5 with in w range [0.0001; 10000] | 5 with in w range [0.0001; 10000] |
| Approximated as | Oustaloup filter | Oustaloup filter |

Table.8. Fuzzy rules

| e / $\frac{d^{\mu}e}{dt^{\mu}}$ | NL | NM | NS | ZR | PS | PM | PL |
|---|---|---|---|---|---|---|---|
| PL | ZR | PS | PM | PL | PL | PL | PL |
| PM | NS | ZR | PS | PM | PL | PL | PL |
| PS | NM | NS | ZR | PS | PM | PL | PL |
| ZR | NL | NM | NS | ZR | PS | PM | PL |
| NS | NL | NL | NM | NS | ZR | PS | PM |
| NM | NL | NL | NL | NM | NS | ZR | PS |
| NL | NL | NL | NL | NL | NM | NS | ZR |

Case 0

Case 1

Case 2

Case 3

Case 4

## 6. SIMULATION RESULTS AND COMPARISON

### 6.1 COMPARING STEP RESPONSES

In this section, 3 controllers are compared with respect to step response, path following and investigation of situation in presence of noise and disturbances. Bogacki-Shampine with fixed step size of 0.001 is considered as differential equation solver. Also meter unit in vertical axes and simulation time with sec. unit in horizontal axes have been used in all of the Figures 11-16. Note that classical PID controller is tuned according to SIMULINK2014b. At first, for initial assessment of step response in three methods, 3 step responses are illustrated in Figure.11. AFFOPID achieves 9.35% improvement in overshoot (OV) in comparison with FOPID. Difference between rise time of classical tuned PID and both FOPID and AFFOPID is significant. As we can be seen in Figure.12, treatments of FOPID and AFFOPID in channel Z are very close and almost match each other; however, they are considerably distant from classical PID controller. The improvement of AFFOPID comparing to FOPID in channel Z in step response is not very impressive and their responses are very close (Figure.12).

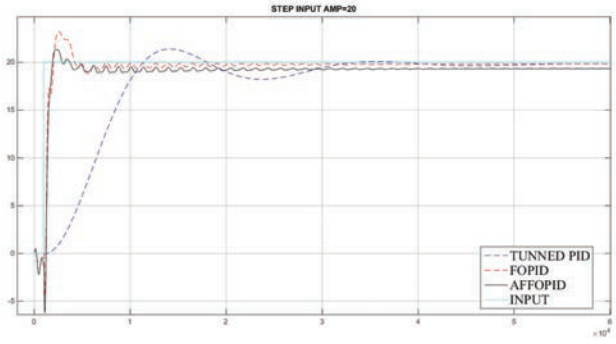


Figure.11. Step response in PID,FOPID and AFFPIDC in channel Y

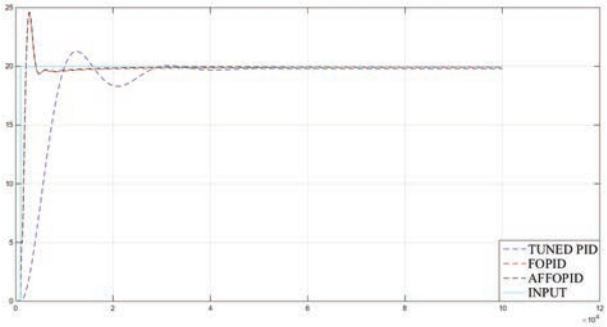


Figure.12. Step response and comparing controllers in channel *Z*

According to Figure.12, AFFOPID obtains 15.85% improvement in overshoot comparing to FOPID while rise time difference is significant.

### 6.2 ENCOUNTERING NOISE AND DISTURBANCE

It's obvious that in AUV case tacking of a pulse is more difficult than other trajectories like sine or ramp; thus, in simulations input pulse is considered. In the following the reaction of 3 controllers while encouter noise and disturbance during trajectory following is investigated.

Figure.13 shows encountering disturbance, the differences between tuned classical PID and two others (FOPID and AFFOPID) is significant and this difference is not comparable. In this case the treatment of traditional PID is very weak and the improvement made by AFFOPID in overshoot comparing to FOPID is about %30.25 while undershoot is improved by %42.45. In this case big disturbances are in the pulse form in 3 discrete times((t= [0~50] Amp=30), (t= [200~250] Amp=-40) and ((t= [400~500] Amp=20)). If we pay attention to input disturbances, we can see that the amplitude of disturbances compared to our trajectory (input=20m) is considerable, but AFFOPID and FOPID compensate this big disturbance and PID has not a good treatment at all. cafully examining the

figure, one may find out that AFFOPID is much better than FOPID in response (%30.25).

Figure.14 shows that the rise time in classical PID is much bigger than two other controllers and noise cancelation is about %9.35 weaker than AFFOPID and FOPID. Moreover, in PID improper treatment of undershoot and overshoot is clear. In this case the improvement of AFFOPID compared to FOPID is minor according to Figure.14(b). Furthermore, the transient response of PID is not appropriate in comparison with other controllers.

According to Figure.15 comparing noise cancelation in channel z, AFFOPID is better than FOPID but these are better than classical PID about %13.42. As can be seen in Figure.15, in fact PID controller does not paly a considerable role in noise cancelation in contrast with two other controllers.

Similarly, Figure.16 shows that the noise cancelation in channel Y obtained by PID is very weak in comparison with two other controllers. AFFOPID has lower overshoot compared to FOPID (about %9.4) but to some extend the transient response has more fluctuations comparing to FOPID.

## 7. CONCLUSION

In this paper, first off, a comprehensive nonlinear model of AUV was derived and verified. The doubled PID controller was implemented based on derived plan and tracking on desired trajectory in 3 dimensions was done simultaneously. In proposed approach, two new controllers AFFOPID and FOPID implemented on linearized model in channel Yand Z simultaneously. The special fuzzy strategy helps coefficients of controller be online and makes the system adaptive. In this way, deriving the exact model of system is not necessary. The performance of the proposed controller was investigated. The simulation results revealed that this new controller has a good treatment when encountering high noise and vast disturbance. The results demonstrated that robustness and adaptivety requirements were properly fulfilled. The improvement in over shoot, undershoot, noise cancelation, resistance against disturbances and error of steady state was significant. In this study the requirment for implemetation in realistic conditions was considered. Replacing fuzzy part with a type2 fuzzy may constitute future reseach work. In this way, the significance of uncertainty in AUV modeling is reduced and robustness is improved.

## 8. REFERENCES


1. FARRELL, J. A., PANG, S., LI., W. and ARRIETA, R. “Biologically Inspired Chemical Plume Tracing Demonstrated on an Autonomous Underwater Vehicle”, *Man, and Cybernetics Conference, Hague, Netherlands*, September 2004.
2. YILDIZ, O., GOKALP, R.B. and YILMAZ, A.E. “A review on motion control of the Underwater Vehicles,” in proc. *Electrical and Electronics Engineering, 2009. ELECO 2009, Bursa, 2009*, pp. II-337-II-341.
3. UUV programs, http://ftp.fas.org/irp/program/collect/uuv.htm, September 2007.
4. PRESTERO, T. “Verification of a Six-Degree-of-Freedom Simulation Model for the REMUS Autonomous Underwater Vehicle”, *MSc/ME Thesis, Massachusetts Institute of Technology,* September 2001.
5. GEISBERT, J.S. Hydrodynamic Modeling for Autonomous Underwater Vehicles Using Computational and Semi-Empirical Methods. *Verginia Polytechnis Institute and State University, 2007; Key Information: Kinematic model, Dynamic model.*
6. YUE, C., GUO, S. and LI, M. “ANSYS FLUENT-based modeling and hydrodynamic analysis for a spherical Underwater robot”, *Proceedings of 2012 IEEE International Conference on Mechatronics and Automation*, pp. 1577-1581, 2012.
7. GUO, S., MAO, S., SHI, L. and LI, M. “Design and Kinematic analysis of an amphibious spherical robot”, *Proceedings of 2012 IEEE International Conference on Mechatronics and Automation,* pp. 2214-2219, 2012.
8. HERMAN, P. “Decoupled PD set-point controller for underwater vehicles,” *Journal of Ocean Engineering, vol. 36, no. 6-7*, pp. 529-534, May 2009.
9. YILDIZ, O., GOKALP, R.B. and YILMAZ, A.E. “A review on motion control of the Underwater Vehicles," in proc. *Electrical and Electronics Engineering, 2009. ELECO 2009, Bursa, 2009*, pp. II-337-II-341.
10. COPELAND, B. R “The Design of PID Controllers using Ziegler Nichols Tuning” March 2008.
11. BUCKHAM, B. J., PODHORODESKI, R. P. and SOYLU, S. “A chattering-free sliding-mode controller for underwater vehicles with faulttolerant infinity-norm thrust allocation," *Journal of Ocean Engineering, vol. 35, no. 16*, pp. 1647-1659, November 2008.
12. ANTONELLI, G., FOSSEN, T. I. and YOERGER, D. R. Underwater robotics. *Springer Handbook of Robotics*, 2008.
13. ZEINALI, M. and NOTASH, L. “Adaptive sliding mode control with uncertainty estimator for robot manipulators”, *Mechanism and Machine Theory, vol. 45, no. 1*, pp. 80-90, January 2010.

14. JUN, S. W., KIM, D. W. and LEE, H. J. "Design of T-S fuzzy-model-based controller for depth control of autonomous underwater vehicles with parametric uncertainties," in *2011 11th International Conference on Control, Automation and Systems, ICCAS 2011, October 26, 2011 -October 29, 2011, Gyeonggi-do, Korea, Republic of*, 2011, pp. 1682-1684.
15. KUMAR, N., PANWAR, V., SUKAVANAM, N., SHARMA, S.P. and BORM, J.H. "Neural network-based nonlinear tracking control of kinematically redundant robot manipulators", *Mathematical and Computer Modelling, vol. 53, no. 9-10*, pp. 1889-1901, May 2011.
16. SUN, T., PEI, H., PAN, Y., ZHOU, H. and ZHANG, C. "Neural network-based sliding mode adaptive control for robot manipulators", *Neurocomputing, vol. 74, no. 14-15*, pp. 2377-2384, July 2011.
17. LIANG, X., GAN, Y. and WAN, L. "Motion Controller for Autonomous Underwater Vehicle Based on Parallel Neural Network", *JDCTA, AICIT, vol. 4, no. 9*, pp. 61-67, 2010.
18. MEDAGODA, L. and WILLIAMS, S.B. Model predictive control of an autonomous underwater vehicle in an in situestimated water current pro_le. *In OCEANS, 2012 - Yeosu*, pages 1{8, 2012.
19. STEENSON, L. V. Experimentally Veri_ed Model Predictive Control of a Hover-Capable AUV. *PhD thesis, University of Southampton*, 2013.
20. WANG, L. Model Predictive Control System Design and Implementation Using MATLAB. *Springer Verlag*, 2010.
21. STEENSON, L.V., PHILLIPS, A.B., TURNOCK, S.R., FURLONG, M.E. and ROGERS, E., "Effect of measurement noise on the performance of a depth and pitch controller using the model predictive control method" *Autonomous Underwater Vehicles (AUV), 2012 IEEE/OES ,* vol., no.,pp.1,8, 24-27 Sept. 2012.
22. Advanced control of autonomous underwater vehicle by Dr of philosophy in mechanical engineering 'side Zhao' in August 2004.
23. PILTAN, F., ARYANFAR, A. H., SULAIMAN, N. B., MARHABAN, M. H. and RAMLI, R. "Design Adaptive Fuzzy Robust Controllers for Robot Manipulator", *World Applied Science Journal, vol. 12, no. 12,* (2011), pp. 2317-2329.
24. BENCHOHRA, M. and BOUTEFAL, Z. Impulsive Differential Equations of Fractional Order with Indefinite Delay, *Journal of Fractional Calculus and Applications, Vol. 5*. July 2013, No. 5, pp. 1-15.
25. CHANG, X.. JIANHONG, L. and MING, C et al. Neural network PID adaptive control and its application[J]. *Control Engineering of China, 2007, 14(3): 284-286 (in Chinese)*.
26. MONJE, C. A., CHEN, Y. Q., XUE, D., VINAGRE, B. M. and FELIU, V. "Fractional-order systems and control: fundamentals and applications", *Advances in Industrial Control, Springer,* 2010.
27. SGARIOTO, D. "Steady State Trim and Open Loop Stability Analysis for the REMUS Autonomous Underwater Vehicle", *Defense Technology Agency, New Zealand Defense Force, DTA Report 254,* March 2008.
28. YANG, C "modular modeling and control for autonomous underwater vehicle (AUV)" *thesis of master of engineering department of mechanical engineering national university of Singapore* 2007.
29. LIN, F.C. "Adaptive fuzzy logic-based velocity observer for servo motor drives." *Mechatronics, 13:229-241*, 2003.
30. LEE, C-H and CHANG, F-K "Fractional-order PID controller optimization via improved electromagnetism-like algorithm", *Expert Systems with Applications, Volume 37, Issue 12*, pp. 8871-8878, December 2010.
31. Model based predictive control of AUVS for station keeping in a shallow water wave environment. 2005 *Naval Postgraduate School, Center for AUV search,Monterey,CA,93943-5000.* 2005
32. DAS, S., SAHA, S., DAS, S and GUPTA, A. "On the selection of tuning methodology of FOPID controllers for the control of higher order processes", *ISA Transactions, Volume 50, Issue 3,* pp. 376-388, July 2011.
33. KRISHNA, B.T. "Studies on fractional order differentiators and integrators: a survey", *Signal Processing, Volume 91, Issue 3,* pp. 386-426, March 2011.
34. DAS, S., PAN, I., DAS, S and GUPTA, A. "A novel fractional order fuzzy PID controller and its optimal time domain tuning based on integral performance indices", *Engineering Applications of Artificial Intelligence,* 2012, 25, 430-442.
35. TEPLJAKOV, A "Fractional-order Calculus based Identification and Control of Linear Dynamic Systems, master thesis", TALLINN 2011.


 

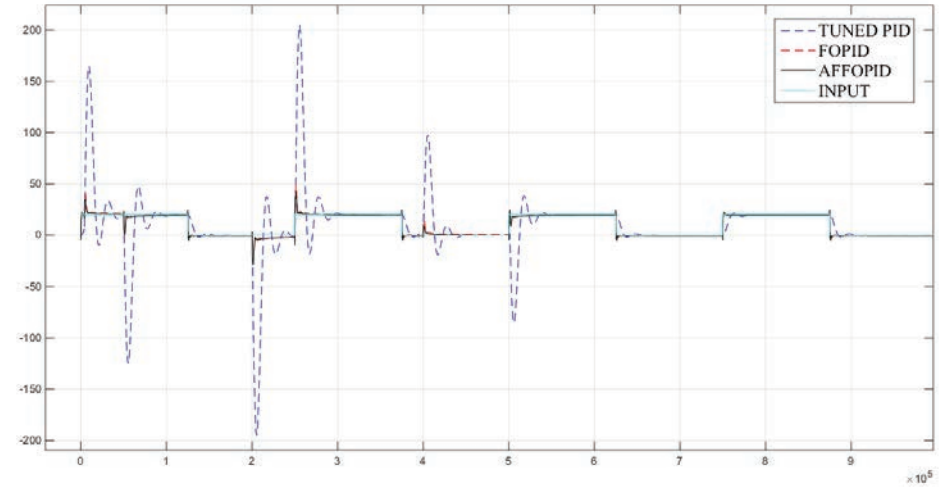


(a)

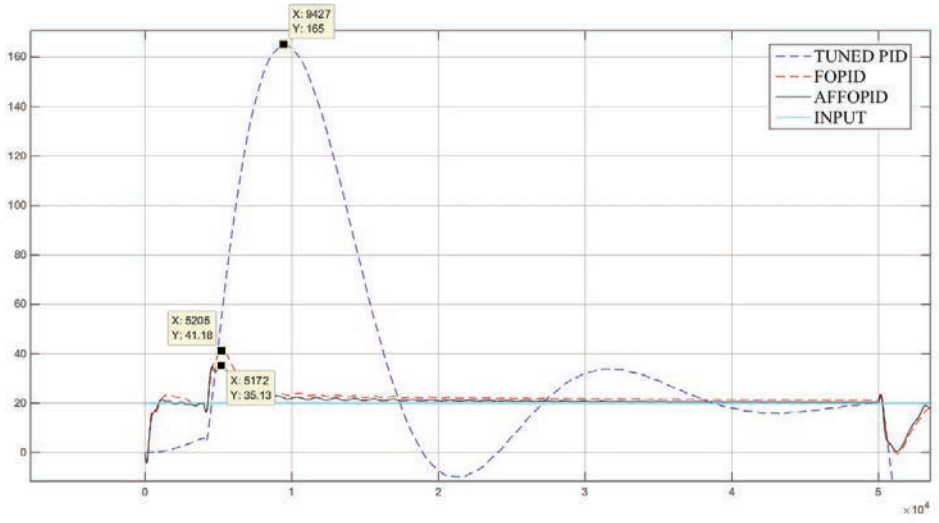


(b)

Figure.13. a) Controller comparison with input Pulse tracking in presence of 3vast discrete disturbances in channel Y. b) Detailed and zoomed version of Figure 13(a) at first part

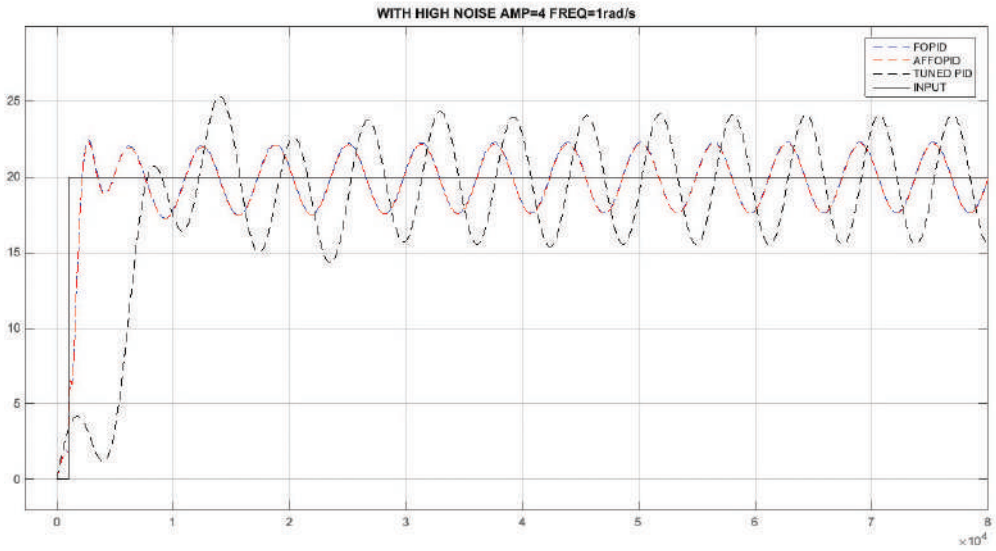


(a)

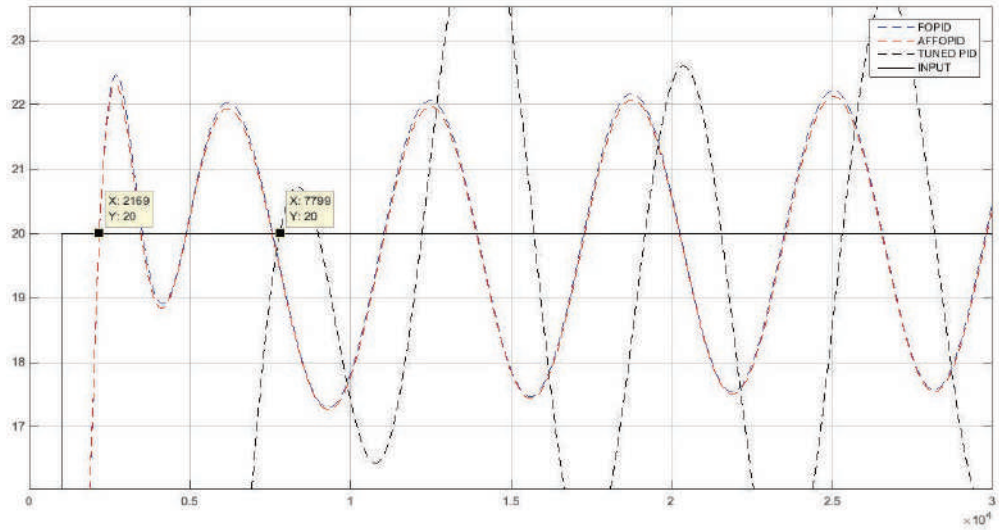


(b)

Figure.14. a) Pulse tracking in channel $z$ in neighbor of high sensor noise entrance (Freq=1rad/s with Amp=4). b) Detail of Figure. 14(a)

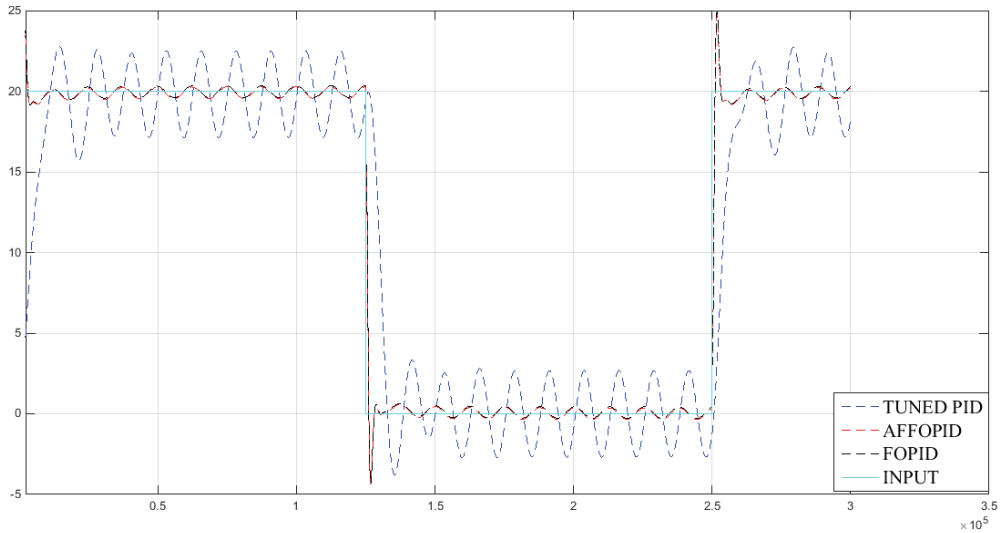


Figure.15. Pulse tracking in channel $\underline{z}$ in neighbor of sensor noise entrance (Freq=0.5rad/s with Amp=4).

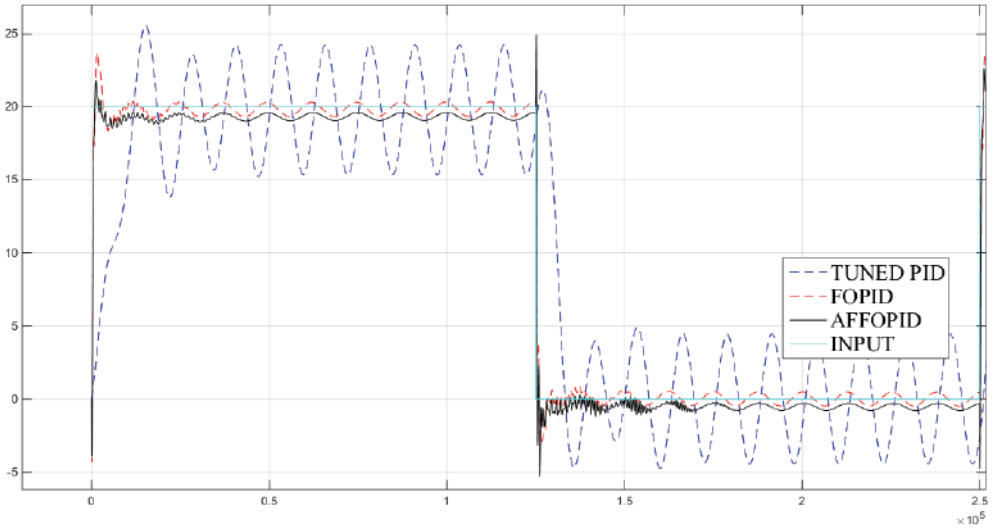


Figure.16. Pulse tracking in channel $\underline{y}$ in presence of sensor noise entrance (Freq=0.5rad/s with Amp=3.5).